Polymer Chemistry

Accepted Manuscript

ROYAL SOCIETY OF CHEMISTRY

www.rsc.org/polymers

Graphical Abstract

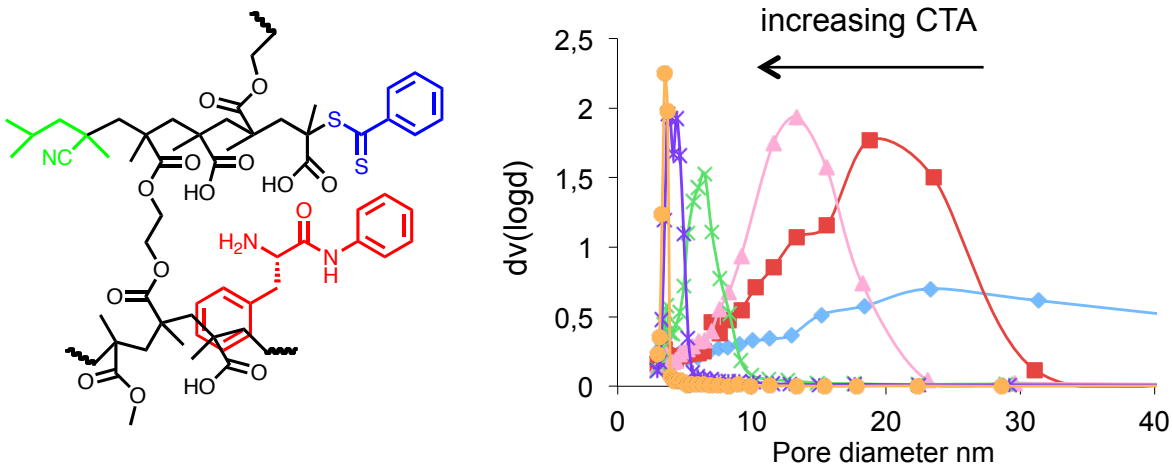

The enhanced performance of molecularly imprinted polymers prepared by controlled radical polymerization in terms of affinity, selectivity, capacity and mass transfer properties is here shown to correlate with pore structure parameters in their dry and swollen state.

Insights into the formation, structural properties and performance of RAFT polymerized L-phenylalanine anilide molecularly imprinted polymers

Mahadeo R. Halhalli[1a] and Börje Sellergren[1,2]

1) Department of Chemistry, TU-Dortmund, Otto Hahn Str. 6, 44221 Dortmund, Germany
2) Department of Biomedical Sciences, Faculty of Health and Society, Malmö University, 20506 Malmö, Sweden. Tel: +46+703-620062, Email: borje.sellergren@mah.se

a) Present address: Product development department, Carl Bechem Lubricants India Private Limited, Bidadi Industrial Area, 562109 Bangalore, India.

Dedicated to the memory of David Sherrington

Abstract

Conventional molecularly imprinted polymers (MIPs) are amorphous materials with a nonuniform microenvironment and a broad distribution of binding sites. Controlled radical polymerization has been demonstrated to improve their properties in this regard. The RAFT method was employed in the present study with the aim of achieving more homogeneous MIP monolithic structures. RAFT control by α-cyanobenzyldithibenzoate was employed during the synthesis of a poly(methacrylic acid-co-ethylene glycol dimethacrylate) conventional MIP for L-phenylalanine anilide. The relationship between polymerization conditions and the structure of the monolith were investigated. The influence of the amount of added RAFT agent on the polymerization as well as on the polymer porous structure and properties was studied. The results demonstrate that the RAFT agent promoted retardation and a more gel-like polymer morphology as reflected in a decrease in pore diameter and an increased swelling factor with added RAFT agent. This was accompanied by an enhanced thermal stability of up to 100°C compared to a corresponding MIP prepared by FRP. The RAFT polymers were then tested in the chromatographic mode for their ability to resolve the racemate D,L-PheNHPh. An optimum RAFT agent level during polymerization was found to result in markedly enhanced selectivity, column efficiency and resolution accompanied by a considerably higher sample load capacity when compared to polymers prepared in absence of RAFT agent.

Introduction

Today molecular imprinting represents an established and versatile concept to generate materials and polymers (MIPs) in various forms exhibiting molecular recognition.[1-4] Applications of such artificial receptors are commonly as antibody substitutes and comprise sensing, separations,

selective preconcentrations and in medicine as drug delivery devices or as therapeutic agents. Free radical polymerization (FRP) is by far the most common technique used to produce such materials mainly because of the compatibility of FRP with a wide range of functional monomers, porogens and template molecules as well as with mild reaction conditions.[5] The major part of the reported MIPs are produced by FRP in concentrated monomer solutions containing a high level of crosslinker. This typically results in amorphous macroreticulate polymers featuring heterogeneity at all length scales. In spite of numerous impressive demonstrations of molecular recognition ability of such materials, they are amorphous in nature and feature a nonuniform distribution of binding sites.[6] This is reflected in nonlinear binding isotherms and a limited saturation capacity.[7] Moreover, mass transfer in such materials is impeded due to a high degree of partly buried binding sites.[8] Part of this problem can be explained in terms of the FRP mechanism which is associated with a fast chain growth, rapid attainment of high molecular weights, high chain polydispersities, intramolecular crosslinking and irreversible termination reactions.[9] This impedes efficient chain relaxation and contribute to network inhomogeneity.

To address this problem we,[10-12 13-15] and others, [16-20 21-24] have investigated means to control FRP-based imprinting through controlled radical polymerization (CRP). The overall lower concentration of active radicals in CRP is accompanied by a slower propagation rate and a suppressed chain termination which in turns results in lower chain polydispersities, defined molecular weights and homogenous network structures.[25-30] Molecularly imprinted networks prepared by CRP have been reported to feature enhanced binding affinity as well as binding capacity.[13, 14, 19, 21-24]

Several CRP techniques have been assessed for improving imprinted polymer networks per se, [13, 19-22, 24] for facilitating grafting or surface initiated polymerizations [10-15, 17, 18] or for the

development of MIP nanoparticles of low dispersity.[23, 31-35] These include mainly ATRP,[17, 18, 20, 31, 35] RAFT,[12-15, 22, 23, 32-34] NMP[16] and Iniferter[10, 11, 23] chain polymerization. Among the CRP techniques RAFT (reversible addition- fragmentation chain transfer) polymerization belongs to the more versatile systems because of its compatibility with a wide range of monomers, templates and solvents and the mild reaction conditions. RAFT polymerization is based on the addition of chain transfer agents (CTAs) of which dithioesters have proven particularly versatile.[36] These serve to cap the majority of the propagating chains followed by the establishment of a dynamic equilibrium between growing and dormant chains.[37] The resulting lowering of the concentration of active radicals leads to a reduced termination by radical recombination, a slower kinetics, and a linear time-conversion curve. Furthermore, interchain equilibration reduces chain length dispersity and network heterogeneity.

Sofar, only few studies have been reported aiming at describing the impact of CRP and particularly RAFT polymerization on the structure, recognitive and mass transfer properties of MIPs.[12, 13, 22, 24] Notably, we are aware of only one study[47] aiming at understanding its impact on the pore structure of porous polymer resins. This appears particularly urgent given the significantly enhanced affinities and saturation capacities that have been reported for such materials. Moreover, the growing importance of CRP for producing novel MIP architectures and imprinted nanoparticles warrants further fundamental studies of this process. The work reported here attempts to correlate recognitive performance with structural properties with a focus on a model representative imprinted polymer resin prepared in presence of a high level of crosslinker.

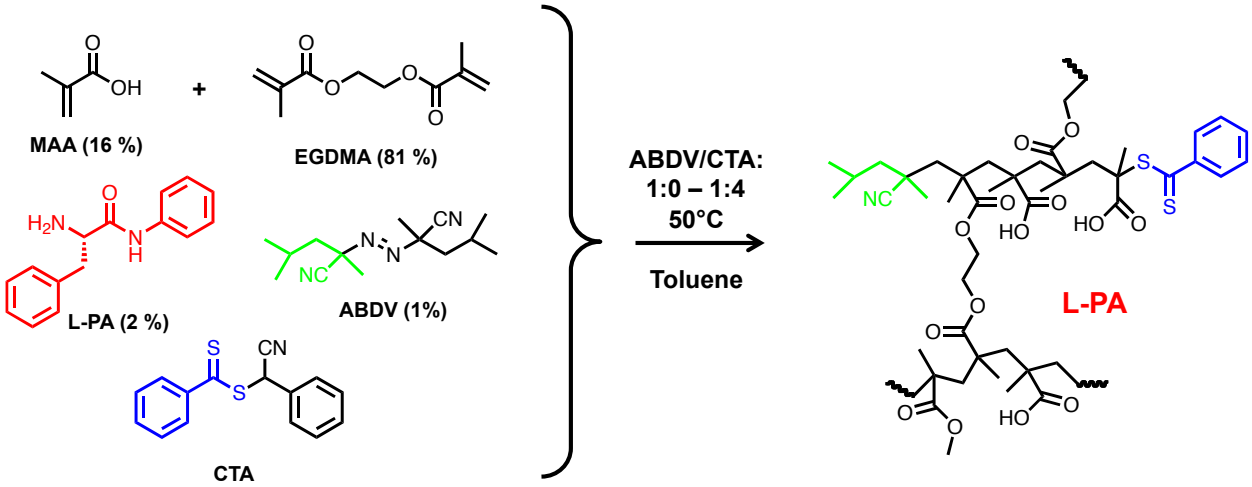

Figure 1. Preparation of L-PA imprinted polymer using RAFT polymerization. The % values are given in mole %.

Experimental section

Chemicals

Methacrylic acid (MAA) and ethyleneglycol dimethacrylate (EGDMA) were obtainded from Aldrich (Deisenhofen, Germany) and purified as reported elsewhere prior to use. [6] 2,2'-Azobis(2,4-dimethylvaleronitril) (ABDV) was purchased from Acros Organics and was recrystallised in methanol before use. The templates L- and D-phenylalanine anilide (L-PA, D-PA) were synthesized following a previously described procedure.[38]

Phenylacetonitrile, N-bromosuccinimide, phenyl magnesium bromide (3M solution in ethyl ether), deuterated chloroform, THF (anhydrous), magnesium sulphate, benzoyl peroxide, carbon disulphide, carbon tetrachloride and toluene (HPLC grade) were acquired from Aldrich (Deisenhofen, Germany) and were used as received. HPLC grade acetonitrile and methanol were purchased from Merck (Darmstadt, Germany). The odorless RAFT chain transfer agent (CTA) (α-Cyanobenzyl Dithibenzoate) was synthesized according to literature procedures.[39]

Apparatus

The HPLC measurements were carried out on an Agilent 1200 series instruments (Agilent Technologies) equipped with a UV diode array detector and an autosampler.

Elemental microanalysis was performed at the Department of Organic Chemistry, Johannes Guttenberg Universität Mainz using a Heraeus CHN-rapid analyser (Hanau, Germany).

Fourier transform infrared (FT-IR) spectroscopy was performed using a NEXUS FT-IR spectrometer (Thermo Electron Corporation, Dreieich, Germany).

The particle morphology was determined using a scanning electron microscope SEM Hitachi S 4500 at the Department of Biochemical and Chemical Engineering, TU Dortmund.

Nitrogen sorption measurements were performed on a Quantachrome (Nova 4000e surface area and pore size analyzer) automatic adsorption instrument. Prior to measurements,100-150 mg of the samples was heated at 40 °C under high vacuum (10^{-5} Pa) for overnight. The specific surface areas (*S*) were evaluated using the BET method, the specific pore volumes (*V*p) were evaluated following the Gurvitch method, and the average pore diameter (*d*p) was evaluated using the BJH theory.

Thermogravimetric analysis and isothermal curing kinetics were performed using a TGA Q_{50} and a DSC Q_{200} instrument respectively (TA instruments, Eschborn, Germany).

Synthesis of α-bromobenzene acetonitrile

Phenylacetonitrile (1.0 g, 8.53 x 10^{-3} mol), N-bromosuccinimide (1,6 g, 8.53 x 10^{-3} mol) and benzoylperoxide (0.01 g, 4.13 x 10^{-5} mol), were refluxed in dry carbon tetrachloride (10.0 mL) for 6 hours. The product was cooled and filtered and the solvent was removed under vacuum. The product was purified through a silica column (hexane:diethyl ether, 70:30). The product was obtained as yellow oil (40 %). ^{1}H NMR (CDCl3) δ (PPM): 5.50 (s, 1H,

C(CN)*H*(C6H5)), 7.43-7.46 (m, 3H,Ar*H*), 7.55-7.58(m, 2H, Ar*H*). **^{13}C** NMR (CDCl3) δ (PPM): 27.4, 116.4, 127.8, 128.9, 129.5, 129.8, 130.4

Synthesis of α-Cyanobenzyl Dithibenzoate (CTA)

Phenylmagnesium bromide (3M solution in ethyl ether) was diluted to 20ml with anhydrous THF. Carbon disulphide (1.2 g) was added dropwise to this mixture, and the mixture was stirred for 0.5h at room temperature. To the dark red solution was added drop wise 3g of alpha-bromobenzene acetonitrile, and the mixture was stirred for another 3h. Water was added to the mixture, and organic product was extracted with diethyl ether (3x 50ml), dried with magnesium sulfate overnight and filtered. After the removal of the solvent and column chromatography (3:1 mixture of hexane and ethyl ether), pure product was obtained as a red, odourless solid (70% yield). ^{1}H NMR (CDCl3) δ (PPM): 6.06(s,1H,C(S)SC(CN)H), 7.40-7.47(m,5H,ArH), 7.55-7.61(m,3H,ArH), 7.98-8.00(d,2H,ArH). ^{13}C-NMR ($CDCl_3$): 43.33, 116.59, 117.08, 127.42, 128.08, 128.47,129.04, 129.78, 130.77, 133.83, 143.44, 222.71.

General Polymerisation Procedure

MAA (0.34mL; 4 mmol), L-phenylalanine anilide (L-PA) (120mg; 0.5 mmol) and EGDMA (3.8 mL; 20mmol) were dissolved in 5.7 ml toluene in a 20 mL glass scintillation vial followed by addition of ABDV (62.1mg; 0.25 mmol) and the CTA. The mixture was transferred to a 50 mL glass polymerisation tube. This was degassed with nitrogen for 10 minutes and flame sealed. The thermally initiated polymerisation was done at 50 $^{\circ}$C for 24 h and further curing was carried out at 70°C for 24 h in an oil bath. After 48h the tubes were crushed and the polymers ground in a mortar, followed by Soxhlet extraction in methanol and formic acid (80/20 v/v) for 24 h followed by 24 h in methanol. The polymers were dried under vacuum at 40 ^{0}C overnight

and sieved to a grain size fraction of 25-50 μm. Non-imprinted polymers (NIPs) were prepared identically but in absence of template.

HPLC Measurements

The polymers were slurry packed into stainless steel columns (4.6 x 35 mm (i.d. x l), Merck, Darmstadt, Germany) using MeOH/H_2O : 80/20(v/v) as pushing solvent and evaluated chromatographically. The flow rate was adjusted to 0.5mL/min and 10μL aliquots of 0.5 mM solutions of pure enantiomers or racemate were injected using MeCN-0.01M sodium acetate buffer, pH 4.8 (9:1) as mobile phase unless otherwise mentioned. The elution was monitored at 260nm. The retention factors (k_L and k_D) and the separation factor (α) were calculated using the following formulae: $k_L=(t_L-t_O)/t_O$; $k_D=(t_D-t_O)/t_O$; $\alpha=k_L/k_D$ where t_L is the retention time of the L-enantiomer, t_D is the retention time of the D-enantiomer and t_O is the retention time of the void marker, acetone.

The elution profiles were also evaluated with respect to the number of theoretical plates (N) and the resolution factor (R_S) as follows:

(1) $$N_D = 16\left(\frac{t_D}{W_{bD}}\right)^2 \text{ and } N_L = 16\left(\frac{t_L}{W_{bL}}\right)^2$$

(2) $$R_S = \frac{2(t_L - t_D)}{w_{bL} - w_{bD}}$$

where t= retention time of the D or L enantiomer and w_{bD} and w_{bL} are the width at the baseline of the D-PA and L-PA peaks respectively.

Batch Rebinding experiment:

Samples (10 mg) of the L-PA MIP were weighed and placed in HPLC vials. Solutions of D- or L-PA (C= 0.05-5mM) in acetonitrile (1 mL) were then added and the suspensions allowed to

incubate for 24 h. Aliquots (30 µL) of the supernatants were then diluted with 270 µL water and transferred to HPLC vials for measurement of the free concentration of PA by HPLC using MeOH/H_2O (0.2% TFA): 62/38 (v/v) as mobile phase and UV detection at 260 nm. The resulting peak areas were used to calculate the amount of polymer bound analyte. Each data point is based on the average of two replicate measurements. Non-linear fitting of theoretical isotherms to experimental data was performed using Sigmaplot software and best fits were evaluated with the Fisher test where a higher F-value indicates a better fit.[40] The adsorption isotherm models evaluated were Langmuir (Eq. 3), Bi-Langmuir (Eq. 4) and Freundlich (Eq. 5).

(3) $q^* = q_s bC/(1+bC)$

(4) $q^* = q_{s1} b_1 C/(1+b_1 C) + q_{s2} b_2 C/(1+b_2 C)$

(5) $q^* = aC^m$

where q* is the concentration of solute in the stationary phase at equilibrium with free solute of concentration C. The Langmuir models (eqs. 3-4) assume that one (eq.3) or two (eq.4) distinguishable classes of sites are present on the surface, each with saturation capacity q_s and association constant b. The dissociation constant K_d was calculated as the inverse of b. The Freundlich isotherm (eq. 5), on the other hand, assumes sites with a Gaussian distribution of binding strengths. Here the width of the Gaussian distribution describes the degree of heterogeneity, through the index m.

DSC and TGA investigations:

Approximately 8 mg (8 µL) of the reaction mixture was placed in hermetically sealed aluminium sample pans and the DSC cell purged with ultra high purity nitrogen for 5 min before

equilibration at the reaction temperature. The experiments were then performed by maintaining a nitrogen flow rate of 50 ml/min to prevent intervention by oxygen. Dynamic scanning was carried out using a heating rate of 10 °C/min and the heat flow (dH/dt) evolving from the exothermic reaction measured as a function of time. The double bond conversion was calculated from equation 6.[41]

(6) $$X = \Delta H_{dy}/\Delta H_0$$

where ΔH_{dy} is the reaction heat generated during a dynamic scan per mole unsaturation and ΔH_0 is the theoretical enthalpy of the methacrylate double bond (ΔH_0 = 13.1 kcal/mol).

The thermal stability of these polymers was investigated as follows. Polymer samples (10-15 mg) were placed on a platinum pan, which was heated with a heating rate of 10 ^{0}C/min from 25 ^{0}C to 1000 ^{0}C, under N_2 atmosphere while monitoring the % mass loss with respect to temperature.

Swelling Experiments

NMR tubes were filled during intermittent vibrations up to 1 cm (142 µL) with dry polymer particles and solvent (1 mL) added. The particles were allowed to equilibrate in the solvent for 24 h, whereafter the volume of the swollen particles was measured. The volume swelling ratio was calculated according to Equation 7: [6]

(7) $$Swelling\ ratio = \frac{bed\ volume\ of\ wet\ particles}{bed\ volume\ of\ dry\ particles}$$

Thermoporometry

Polymer samples (1–2 mg) immersed in solvent were placed in the DSC hermetic aluminum pans and quenched at -60 ^{0}C. The solvent melting behavior was measured by DSC using a 5 $^\circ$C/min scanning rate.

From the DSC curves the melting point depression $\Delta T = T - T_0$ was calculated where T_0 is the melting point of pure acetonitrile = -46 ± 0.3 ^{0}C. Linear regression yields the following numerical expression relating the pore radius (Rp) with ΔT.

(8) $$Rp\ (Å) = -309/\Delta T + 13.$$

Where the Y-intercept represents the thickness in Ångstrom of the solvent layer remaining adsorbed on the internal pore surface (non-freezable solvent).

Inverse size exclusion chromatography (ISEC)

A series of polystyrene standards (Polymer Standards Service, Mainz, Germany) of a molecular weight ranging from 162 to 11,100,000 Da in THF (1 mg/mL) were injected on the polymer packed columns using an Agilent 1200 series HPLC instruments (Agilent Technologies) equipped with a UV diode array detector and an autosampler. The ISEC was run using THF as mobile phase at a flow rate of 0.2 ml/min and the standards detected by UV at a wavelength of 254 nm. Acetone was used as a void marker. Data analysis was performed using software (PSS Porocheck) provided by Polymer Standards Service (Mainz, Germany).

Results and Discussion

Reaction analysis by DSC

L-PA-imprinted copolymers of methacrylic acid (MAA) and ethyleneglycol dimethacrylate (EGDMA) were prepared by thermally initiated FRP as shown in Figure 1, using the compositions detailed in Table 1. As CTA we chose α-cyanobenzyl dithibenzoate which was synthesised in two steps as reported by Li and Benicewicz.[39] This CTA is odorless and feature high activity with respect to RAFT polymerization of methacrylate monomers. The effect of

added CTA was first studied by DSC reaction analysis whereby the CTA/initiator ratio was varied from 0/1 to 4/1.

The retarding effect of the CTA on the onset of the polymerisation was first investigated by a dynamic temperature scan of aliquots of the prepolymerization mixtures corresponding to the compositions in Table 1 (Figure 2, Figure S1). As expected, the onset temperature increased with added CTA whereas the DSC curves became narrower – both observations in line with the inhibiting effect of the CTA on the propagation and the resulting extention of the reaction controlled regime.

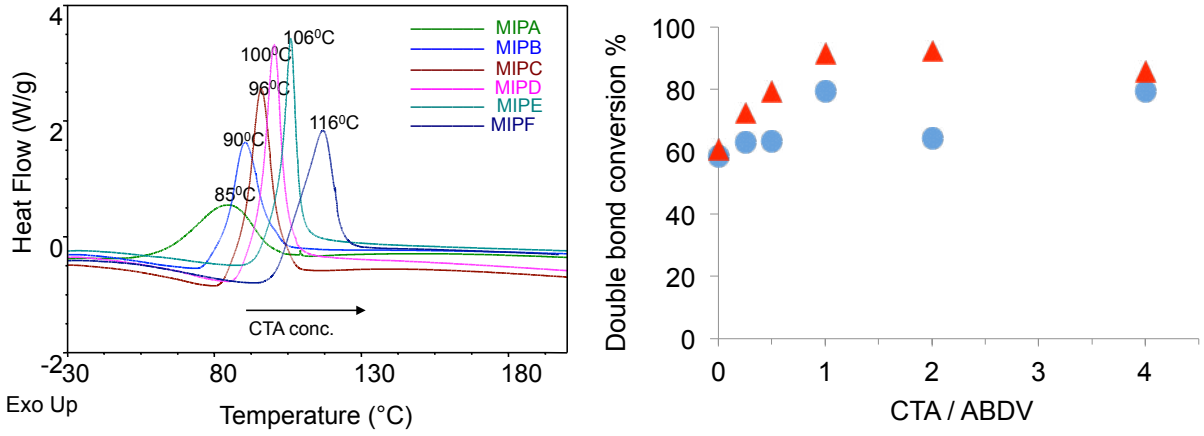

A. B.

Figure 2. (A) Heat generation during a dynamic temperature scan (10°C/min) of the MIP prepolymerisation mixtures corresponding to the compositions in Table 1. (B) Double bond conversion of the imprinted (blue circles) and nonimprinted (red triangles) poly(MAA-co-EGDMA) estimated based on the peak integrals in (A).

The double bond conversion was estimated by dividing the total heat generated per unsaturation with the literature value for the enthalpy of the methacrylate double bond (see experimental section). A conversion of ca 60% in absence of CTA is in rough agreement with the values determined for photoinitiated imprinted networks reported by Byrne et al.[19] and values reported for highly crosslinked macroporous polymers.[42] The poor conversion is due to the high molecular weight dispersity of the primary chains and the restricted mass transfer in the resulting

network. This is alleviated in presence of CTA which contributes to a slower more even chain growth leaving the propagating chain ends and pendent double bonds open and reactive towards the monomers or radicals respectively. This leads to an increased nearly quantitative conversion at a stoichiometric addition of CTA with respect to free radical initiator. The increase is less steep for the L-PA templated networks showing consistently lower conversions compared to the nonimprinted counterparts. As proposed by Byrne et al. we attribute this to an earlier shift from reaction to diffusion controlled growth in presence of template.[22] This is the result of template polymer chain interactions and counteracts the effect of added CTA. The swelling data for the networks further confirms this effect as seen below (Figure 4).

Polymer synthesis and physical characterisation

L-PA imprinted and nonimprinted polymers were synthesised as described in the experimental section and were processed by solvent extraction followed by characterisaiton in the dry state by elemental analysis, optical microscopy, SEM, FTIR and TGA. The pore size analysis in the wet state was thereafter measured by inverse size exclusion chromatography (ISEC) and thermoporometry. Finally batch binding and chromatographic tests were performed in order to investigate the effect of the CTA on chromatographic performance, enantioselectivity and capacity of the materials.

In order to verify incorporation of the RAFT CTA the polymers were visually inspected and subjected to elemental and FTIR spectroscopic analysis. Incorporation of the CTA was visually confirmed by the pink color arising from the dithiobenzoate chromophore with a gradually increasing intensity in proportion to the level of added CTA (Figure S2).

Table 1. Monomer feed composition and pore analysis parameters of the imprinted polymers

Polymer Code	ABDV : CTA (mole/mole)	d_p (nm) [a]	V_p (mL/g) [a]	S (m^2/g) [a]	%S [b]		Yield [b]
					Obt.	Theor.	(%)
A	1 : 0	23	0.69	358	-	-	93 (92)
B	1 : 0.25	19	0.80	389	<0.01 (<0.01)	0.09	99 (92)
C	1 : 0.5	10	0.76	399	<0.01 (<0.01)	0.18	99 (94)
D	1 : 1	6.1	0.43	321	<0.01 (<0.03)	0.37	94 (93)
E	1 : 2	3.7	0.36	323	0.19 (0.17)	0.72	91 (94)
F	1 : 4	3.5	0.23	264	0.43 (0.43)	1.4	89 (86)

a) The BET specific surface area (S), specific pore volume (V_p) and average pore diameter (d_p) of MIPs calculated from the nitrogen adsorption isotherms as described in the experimental part

b) Values in parenthesis refer to nonimprinted polymers.

Surprisingly, as seen in Table 1, this was only partly confirmed by the sulfur analysis. No sulfur was detected for the polymers prepared with CTA/ABDV ratios below or equal to unity whereas only MIPE and MIP F contained detectable sulfur albeit at a ca 3x lower level than expected for a quantitative CTA incorporation. It is known that aromatic dithioesters are relatively unstable and are susceptible to hydrolysis and decomposition. Sulfur may also be lost due to unreacted CTA or CTA incorporation in soluble oligomers. The gravimetric yields showed however that the conversion of monomer to insoluble polymer was nearly quantitative with the exception for the polymers prepared using the high CTA level where the yields dropped below 90%. This indicates an increasing portion of low molecular weight soluble polymer. The FTIR spectra confirmed the successful formation of the expected copolymers with characteristic bands appearing at 1637 cm^{-1} (=C-H bending), 1730 cm-1 (C=O stretch) and 3300-3700 cm-1 (OH stretch) (Figure S3). Moreover, appearance of the C=S bending vibration at 1068 cm-1 is indicative of CTA incorporation.[43] Otherwise the spectra revealed no systematic changes in band intensities with increasing CTA.

Effect of CTA on polymer structure and morphology

The scanning electron micrographs (SEMs) in Figure 3 and Figure S4, reveal the different morphology of the polymers. The polymers prepared using substoichiometric CTA/initiator ratios all showed a macroporous surface texture with clearly visible macropores exceeding 100nm. These are less appearent in MIPC (CTA/ABDV: 0.5/1) and were absent in the polymers prepared using higher ratios (MIPD-F) the latter displaying a smoother surface with smaller pores. This is in agreement with the results reported by Gonzato et al.[24]

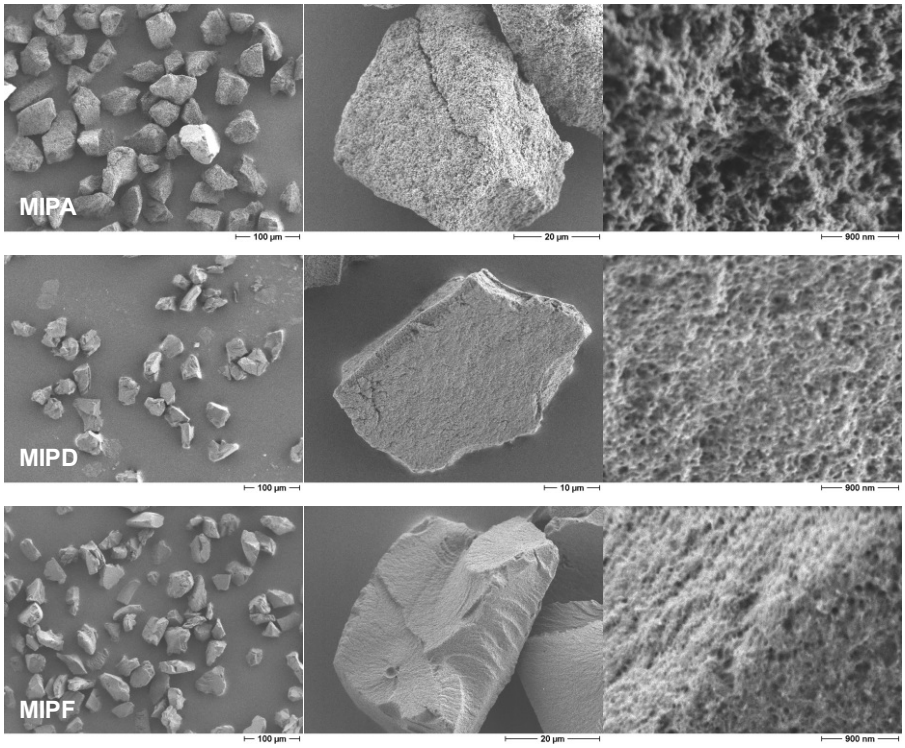

Figure 3. SEM images of the conventional imprinted polymer (MIPA) and RAFT polymers MIP D (CTA/initiator: 1/1) and MIP F(CTA/initiator; 4/1) at three different magnifications.

The decrease in porosity observed with increasing CTA was accompanied by an increased swelling ratio (Figure 4) for the imprinted polymers approaching one unit.

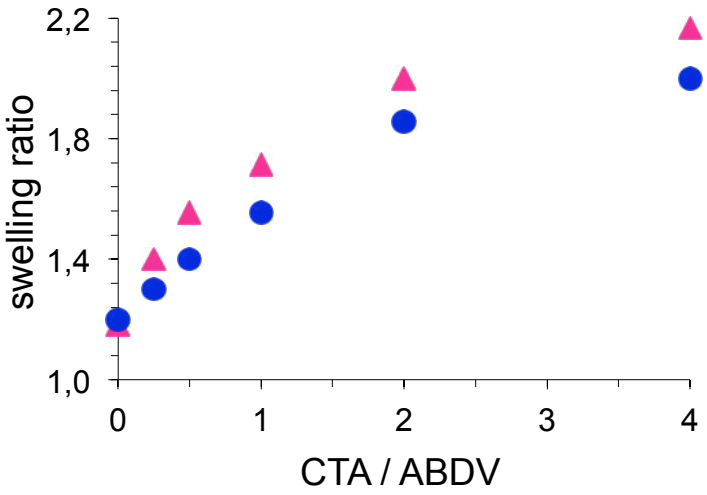

Figure 4. Swelling behaviour of imprinted (red triangle) and non-imprinted (blue circles) polymers in acetonitrile.

The large difference in swelling ratios between the polymers should reflect upon the pore system parameters and we therefore decided to compare the pore systems in the dry and swollen state. The dry pore system parameters were obtained from nitrogen sorption experiments with the isotherms and pore size distributions of the MIP shown in Figure 5 and with associated pore system parameters listed in Table 1 and Table S3 and displayed in Figure 6.

All nitrogen sorption isotherms were of Type IV displaying hysteresis loops indicative of mesoporous materials which is confirmed by the pore system parameters plotted in Figure 6. The presence of CTA however, dramatically influenced the shape of the isotherms. The most significant effect seen in Figure 6 is the continuous shift to smaller more uniform pores with increasing CTA (Figure 5A) whereas the pore volume and surface area displayed a maximum at a CTA/ABDV ratio of 0.5.

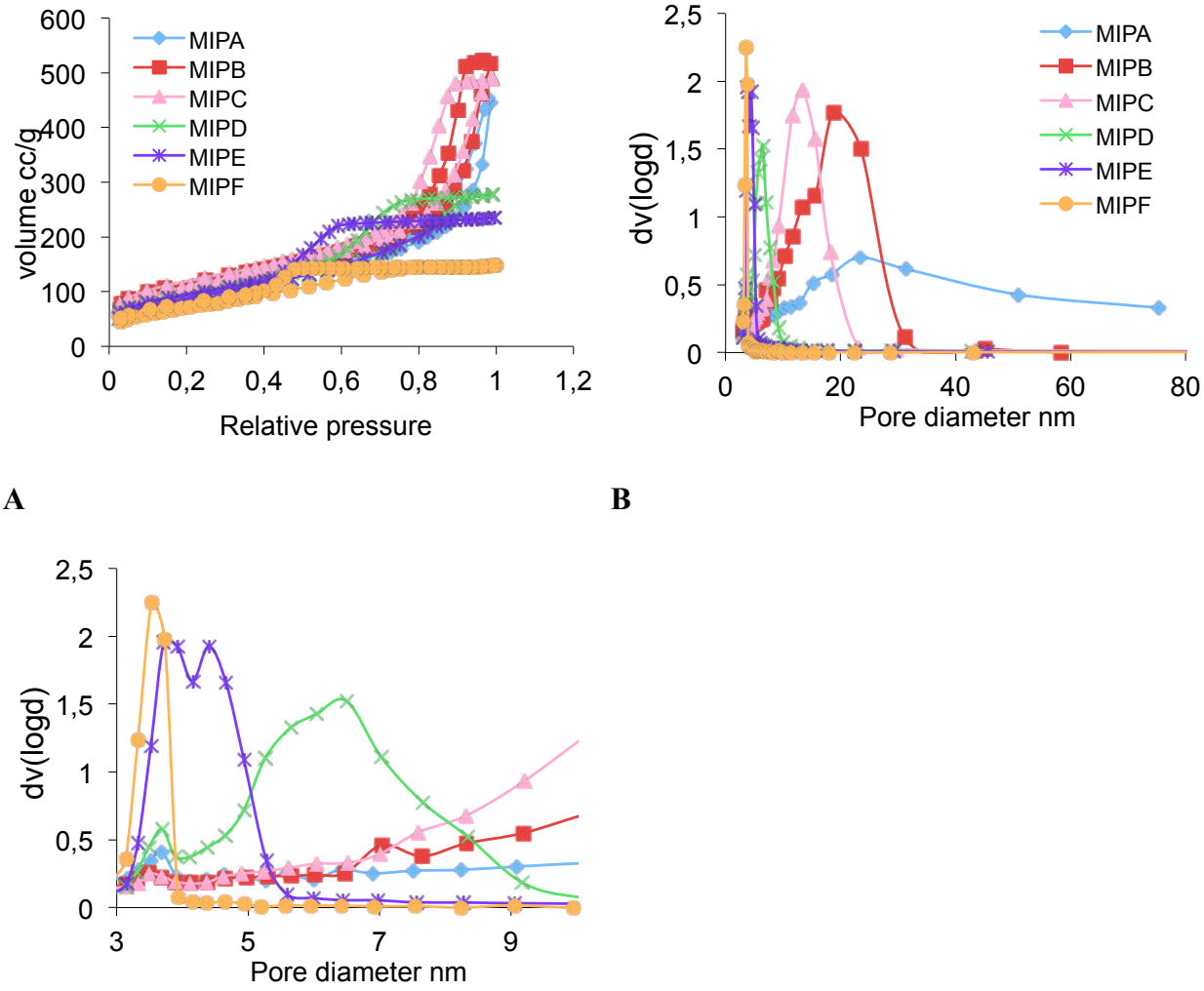

Figure 5. Nitrogen adsorption – desorption isotherms (A) and associated pore size distributions (B and C) of L-PA imprinted polymers prepared using different CTA / initiator ratios.

The reason for the trends observed in Figures 3-6 is not immently obvious but a parallel can be drawn with the morphological effects observed for similar imprinted polymers prepared using solvents of different qualities by either UV- or thermal initiation. As for the polymers prepared in presence of a high level of CTA, the use of solvents which are good at solvating the growing chains extends the reaction controlled regime and delays the phase separation.[42] The microgel particles are small and well solvated resulting in relatively loose particle interconnections and an

open pore system with small pores. The particles are here interconnected by flexible segments leading to a solvent swollen network featuring reversible volume contractions upon drying-soaking. Thus, in the dry state, these polymers are less porous whereas in solution they swell to occupy a volume close to that of a corresponding permanently porous resin. Despite the higher degree of swelling, the extent of unreacted double bonds is lower in these resins (vide supra, Figure 2) indicating that this swelling effect is more caused by the rather loose interconnections than swelling of the microgel particles per se. In these particles, the double bond conversion is high and the consistently higher swelling ratio observed for the MIP resins is probably the result of the lower double bond conversion. UV-initiation is also a means of extending the reaction controlled regime. These polymerizations are typically faster than polymerizations by thermal initiation when comparing identical azo-initiated systems. Due to the faster homolysis of the initiator in the former case, a higher number of propagating chains with a lower average molecular weight can here be expected.

In spite of their gellike swelling behaviour, the polymers prepared in presence of high levels of CTA still feature very high surface areas. Striking is the trend towards narrower pore size distributions which appears clearly for MIPF i.e. the polymer prepared using the highest CTA/ABDV ratio. This contrasts with MIPs prepared by UV-initiation using good solvents which are completely devoid of mesopores in the dry state.[6] Hence shrinking is limited and the materials exhibit permanent porosity at the borderline of meso and microporosity. This shows that the gel particle connectivity is here sufficient to withstand stress caused upon solvent removal, possibly a result of the higher more uniformly distributed crosslinking leading to smaller mesh sizes and a more robust resin.

Further proof for the enhanced robustness was obtained using thermo gravimetric analysis (Figure 7, Table S2). It is evident from the nearly 80°C shift of the 50% mass loss temperature, that the thermal stability increases with increasing CTA/ABDV ratio.

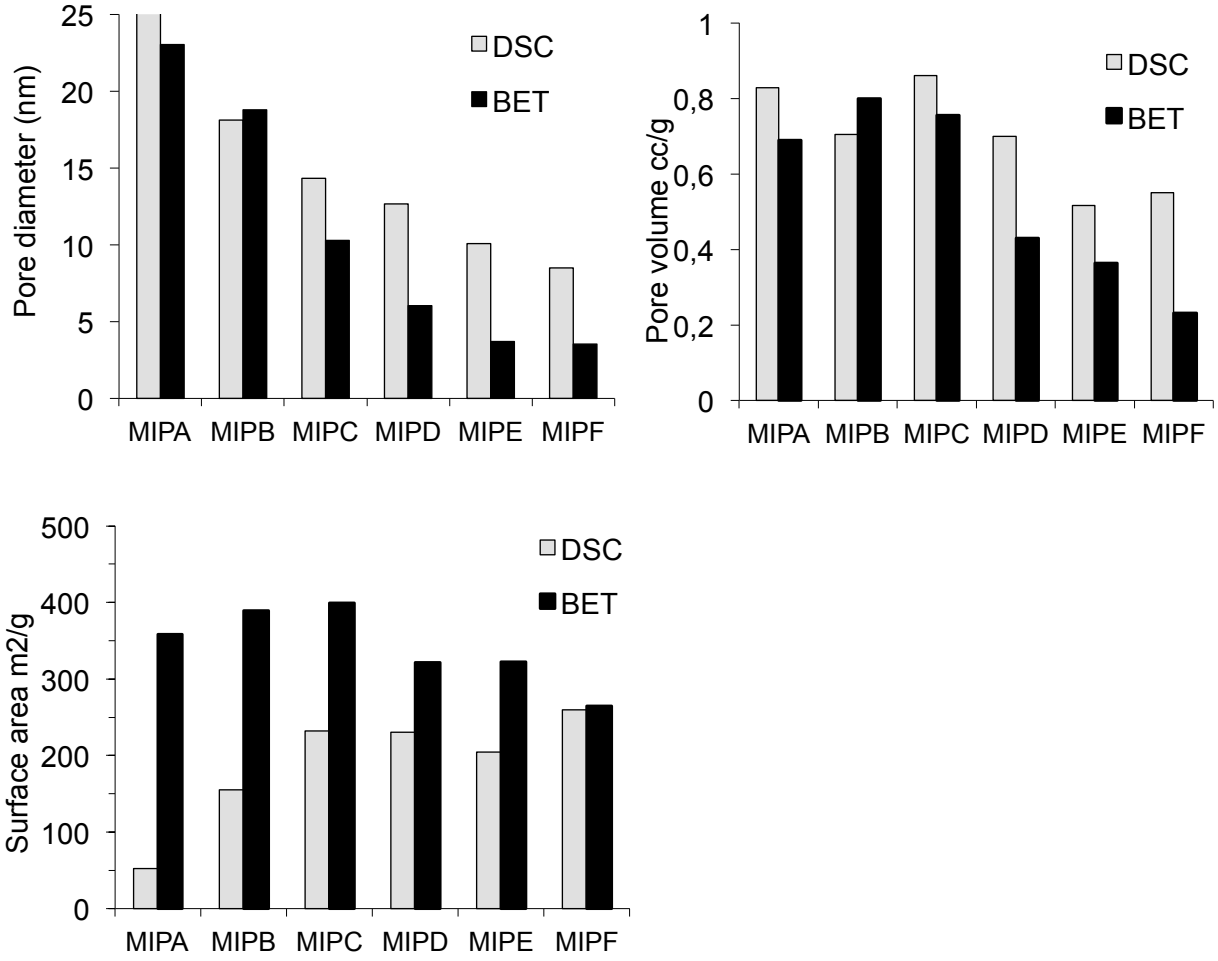

Figure 6. The pore system parameters (A) average pore diameter, (B) pore volume, (C) specific surface area, determined from nitrogen adsorption – desorption isotherms (BET) or thermoporometry (DSC) for the polymers prepared in presence of different levels of CTA.

Moreover whereas the conventional polymers loose mass in two distinct steps (Figure 7B), the mass loss for polymers prepared using high CTA/ABDV ratios occur in one single step. Apart from the more robust particle connectivity a contributing factor may be found considering the mechanistic differencies between FRP and CRP. The former should feature a higher degree of

thermally more unstable head to head bonds since more chains are here terminated by recombination.

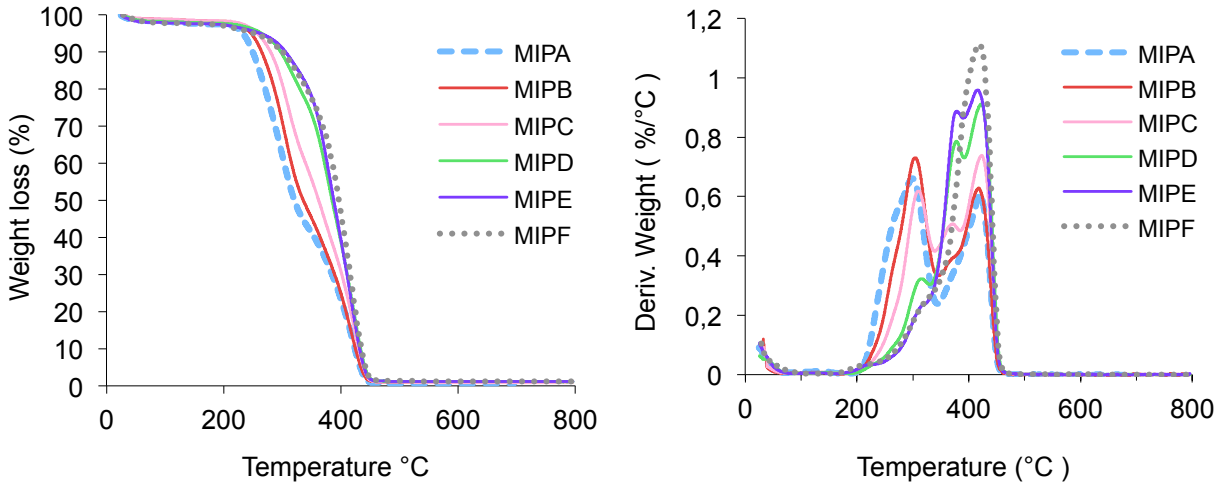

A B

Figure 7. Mass loss curves (A) and their derivatives (B) obtained by thermogravimetry of L-PA imprinted polymers prepared in presence of increasing CTA/initiator ratios in the order A-F.

The above results indicate RAFT mediated FRP to offer a versatile means of tuning the pore size in mesoporous polymers with minor effects on the specific surface area. The high swelling factors measured for these materials warranted a study of their pore system in the swollen state. For this purpose we turned to compare two different techniques, thermoporometry and inverse size exclusion chromatography. Thermoporometry is a calorimetric method for characterising the pore structure of the material from melting or freezing point depression of liquid confined in a pore.[44] Hence, the technique offers valuable insight into the porous properties of a material in its swollen state. The technique is less established than gas sorption since it typically requires calibration and assumes knowledge of surface properties and wetting behaviour of the studied solid and the selection of a suitable solvent.

Moreover the pore sizes that can be accurately determined are limited to pores producing distinct freezing point depressions typically in the size range 2-30 nm.

As can be seen in the DSC thermograms in Figure S5 the melting endotherm peak shifts continuously to lower values with increasing CTA/ABDV ratios, this in agreement with the parallel trend to smaller pore sizes. Based on the Gibbs-Thomson equation and Equation 8 (see experimental section) the freezing point depression can be used to derive the pore diameter and the other pore parameters surface area and pore volume (Figure 6). With the exception of the value for the conventional MIPA prepared in absence of CTA, the difference between the BET and DSC derived pore diameters increases with increasing CTA, hence the difference increases with increasing swelling factor. This results in considerably more gradual decrease in the pore size with increasing CTA and a pore size for MIPE which is more than two times larger than the value determined by the dry state measurement by BET.

ISEC is a chromatographic technique widely used for measurements of the porosity of the polymers in swollen state [45, 46]. It is used to determine the exclusion volume for polystyrene standards of known molecular radii. From the exclusion volumes, the accessible pore volume versus molecular radius can be modelled. As seen in Figure 8 and Table 2, the polymers prepared using a stoichiometric addition of CTA to initiator (MIPD) displayed a significantly narrower pore size distribution compared to the conventional polymer (MIPA). This value is ca two times larger than the dry state value but confirms the general trend identified based on the BET data. The ISEC results are furthermore in close agreement with the pore parameters determined by thermoporometry (DSC). This shows the versatility of both methods as means of gaining swollen state structural information of mesoporous crosslinked networks.

Table 2. Comparison of pore analysis in dry state and swollen state based on three different techniques

code	Dp^a nm	Dp^b nm	Dp^c nm	$V_p{}^a$ cc/g	$V_p{}^b$	$V_p{}^c$	$S_A{}^a$ m^2/g	$S_A{}^b$ m^2/g	$S_A{}^c$ m^2/cm^3	PSD^a width nm	PSD^c width nm
MIPA	23	33	37	0.69	0.83	0.50	358	53	135	50	18
MIPD	6	13	12	0.43	0.69	0.50	321	231	251	2.6	5.5

D_p = Average pore diameter, V_p= pore volume, S_A= Specific surface area, PSD width = width of pore size distribution.

a) Dry state (BET)
b) Swollen state (DSC)
c) Swollen state (ISEC)

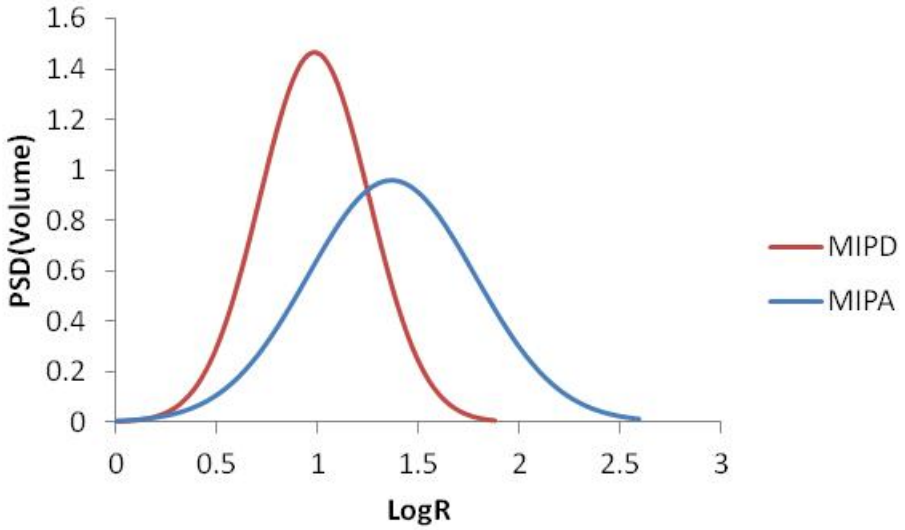

Figure 8. Pore size distribution obtained from ISEC measurements.

Batch binding experiments and chromatographic tests

The question remained whether the dramatic differencies in structure and morphology between the polymers would reflect upon their chromatographic performance and guest recognition properties. Testing of MIPs based on chiral discrimination has here the benefit of specifically probing the cavity contribution to imprinting while cancelling out nonspecific binding

contributions. The polymers were therefore packed in HPLC columns and evaluated chromatographically for their ability to resolve and retain the racemate (D,L-PA) corresponding to the template (L-PA). The resulting elution profiles were evaluated by calculating the retention factors for the two enantiomers (k), the enantiomer separation factor ($\alpha = k_L/k_D$), the number of theoretical plates (N) and the resolution factor (R_s). The parameters for five of the polymers of the series have been plotted in Figure 9. Clearly, addition of CTA has a favorable influence on all parameters up to a point. Hence both the enantio selectivity reflected in the separation factor α, the retentivity k and the column efficiency reflected in the resolution factor R_s and plate number N, increases to pass a maximum at a CTA/ABDV ratio of 1. In the swollen state this polymer features a rather narrow distribution (2-6 nm) of pores averaging 13 nm in size, in contrast with the much broader distribution (ca 50nm) of larger pores averaging ca 35 nm in the non RAFT polymer MIPA. Mass transfer in this more uniform network is facilitated leading to the enhanced performance observed. We subsequently compared the performance of MIPA and MIPD at different sample loads (Figure 10). Also this test came out to MIPD:s favor. Using this column near base line resolution of the racemate was observed up to a sample load of 100 nmol. In contrast no resolution was observed using MIPA at this sample load. In the above discussion we remarked that the RAFT polymerized MIP ressembled a conventional MIP prepared by UV initiated polymerization using a good solvent in terms of pore structure and swelling properties. The ressemblence also holds when comparing the chromatographic properties. As seen in Figure 10 C and D chromatograms obtained from a separate study using bulk polymers independently prepared by UV-initiated polymerization with toluene or dichloromethane (DCM) as porogens displayed striking similarities with the chromatograms in Figure 10 A and B (for the sample load: 10 nmol on column). Dichloromethane is a better solvent than toluene and the corresponding MIP feature a higher chromatographic efficiency (Figure 10D) than a MIP prepared using the

poorer solvent toluene (Figure 10C). This is in analogy with MIPD versus MIPA (Figure 10 A,B).

Equilibrium binding experiments were then performed on MIPA and MIPD and the corresponding NIPs in order to gain insight into the affinity, selectivity and capacity of the MIPs for their template.

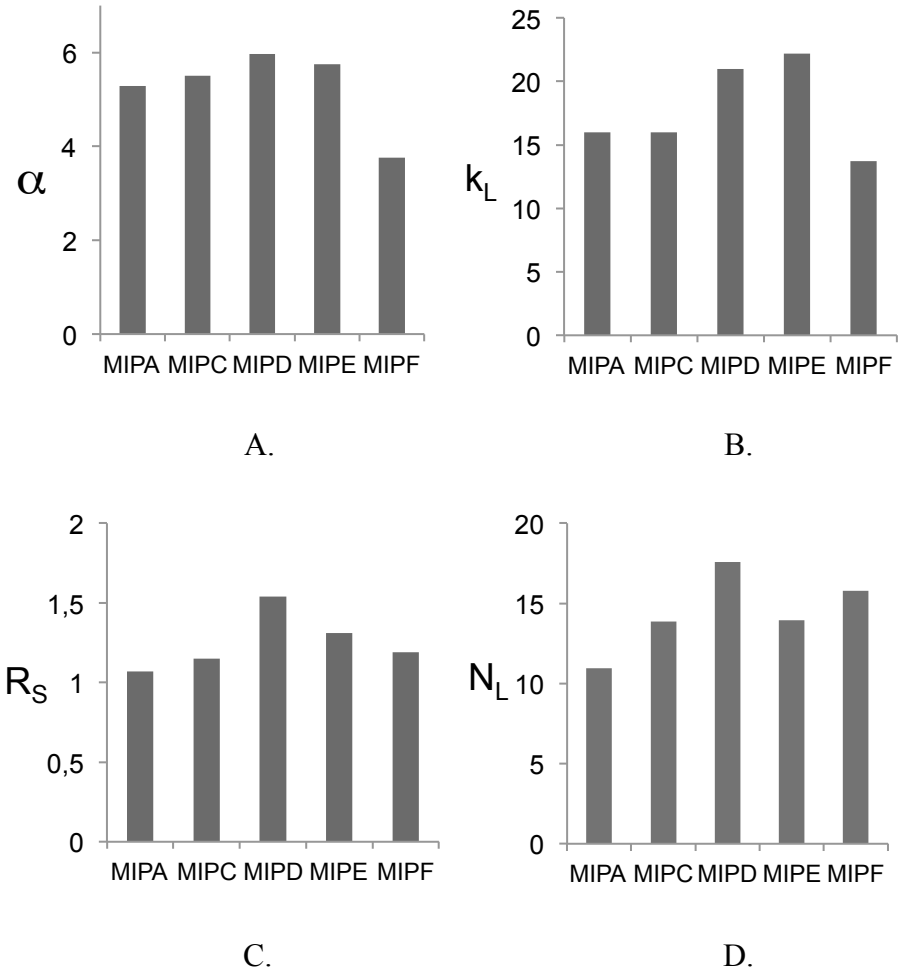

Figure 9. Graphs displaying the separation factor (A), the retention factor for L-PA (B), the resolution factor (C) and the number of theoretical plates for L-PA (D) obtained after injections of D,L-PA (10µL of a 0.5mM stock solution) on columns packed with the indicated polymers. Mobile phase: MeCN-0.01M sodium acetate buffer, pH 4.8 (9:1). Flow rate: 0.5mL/min. Detection: UV absorbance at 260nm.

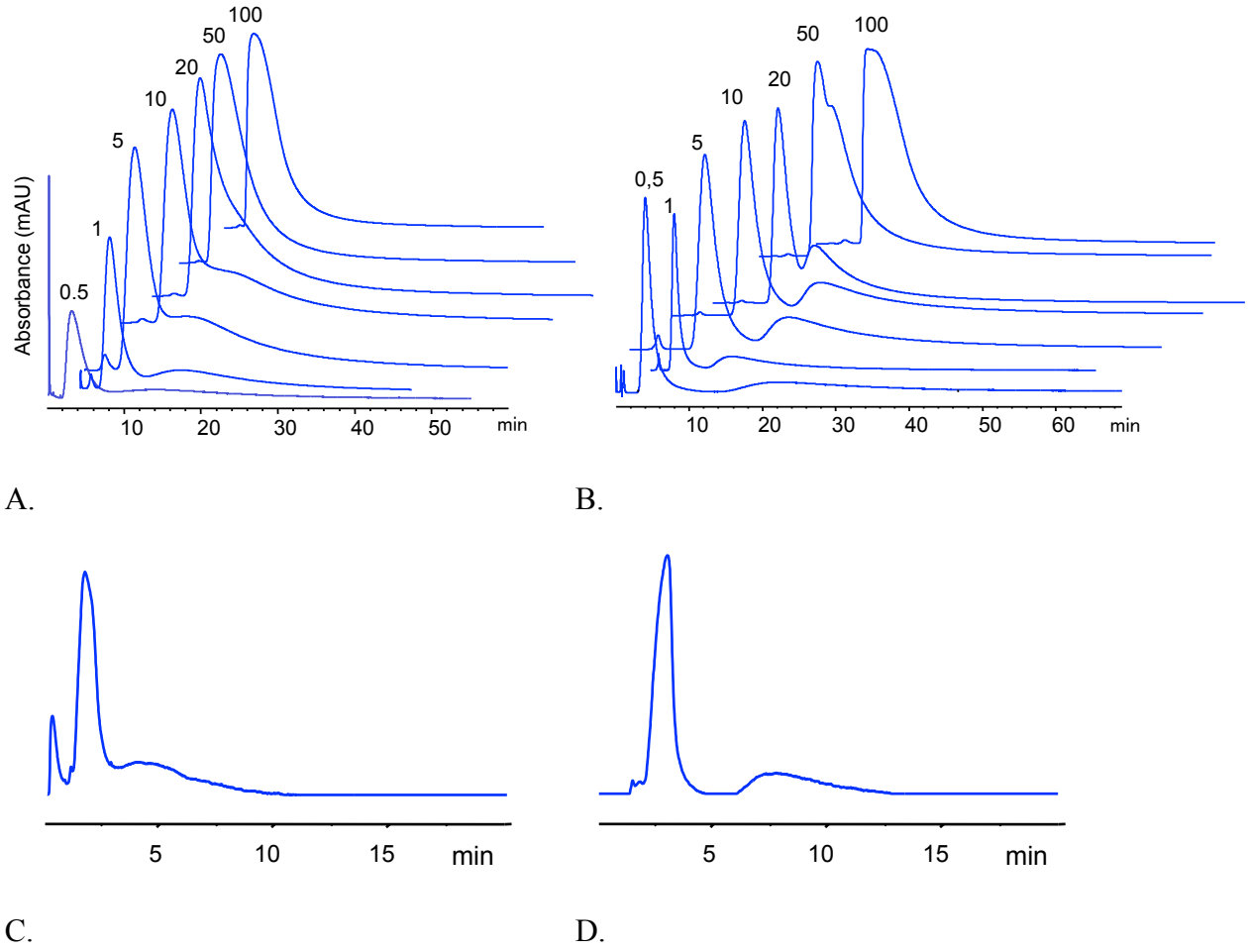

Figure 10. A, B: Elution profiles obtained after injections of D,L-PA (10µL of stock solutions of concentrations (mM) as indicated above each profile) on columns packed with MIPA (A) and MIPD (B) under conditions as indicated in Figure 9. C, D: Elution profiles of D,L-PA (10µL of a 1mM stock solution) on columns packed with conventional bulk MIPs prepared by low temperature UV-initiated polymerization using toluene (C) or dichloromethane (D) as porogens. Mobile phase: Acetonitrile/acetic acid/water: 92.5/5/2.5 (v/v/v). Flow rate: 1 mL/min. Column size: 4.5 x 125 mm2.

Figure 11 shows the binding curves of both enantiomers in acetonitrile for the four polymers and Table 3 the fitting parameters assuming a Langmuir binary site model. As expected only the imprinted polymers display a chiral preference with binding of template L-PA clearly exceeding that of D-PA especially at higher sample loads (> 1mM free concentration). The shape of the curves when comparing MIPA and MIPD are however very different. Whereas MIPA features a

classical hyperbolic curve for L-PA levelling off at ca 47 µmol/g (Table 3), both polymers prepared in presence of CTA (MIPD, NIPD) display steeper binding curves and an overall higher affinity for PA. Only the MIP (MIPD) displays saturation with D-PA (template antipode) leveling off at an uptake of ca 44 µmol/g compared to ca 30 µmol/g for MIPA. In contrast binding of L-PA increases on this polymer continuously attaining an uptake of ca 70 µmol/g at a free concentration of 3 mM. Hence the CTA has a positive influence on both binding capacity and enantioselectivity.

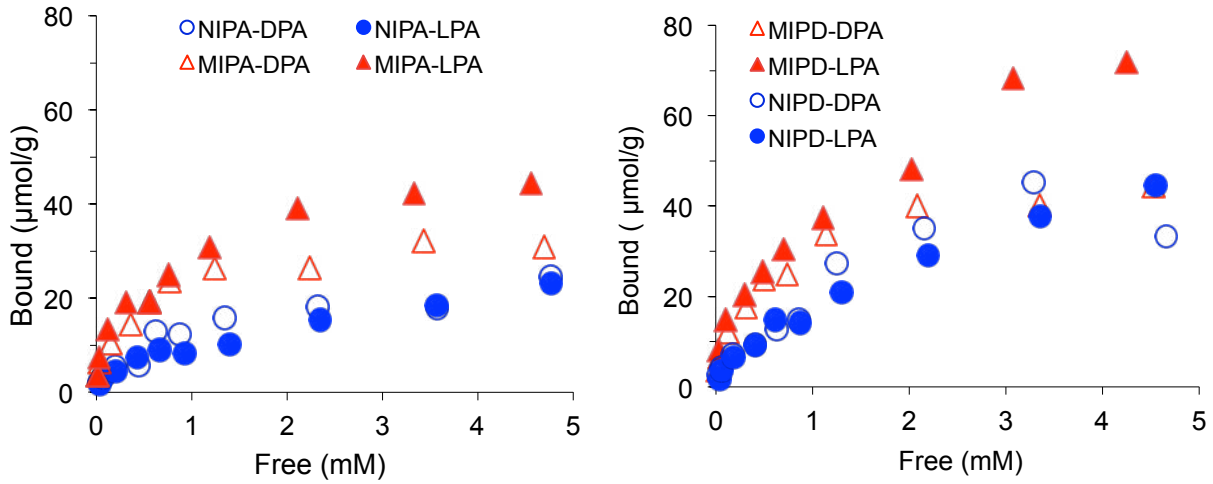

A. B.

Figure 11. Adsorption isotherms of D/L-PA on MIPA (A) and MIPD (B) with corresponding nonimprinted polymer, as solutions in pure acetonitrile

Table 3. Bi-Langmuir Isotherm fitting parameters obtained by nonlinear regression of data shown in Figure 14 as described in the experimental section.

Polymer code		K_d1 (mM)	q_s1 (µmol/g)	K_d2 (mM)	q_s2 (µmol/g)	r^2	F-value
MIPD	L-PA	0.026	15	5.2	131	0.993	746
	D-PA	0.014	6.0	0.8	44	0.993	821
MIPA	L-PA	0.023	11.7	1.8	47	0.992	683
	D-PA	0.005	4.4	0.6	30	0.988	532

Conclusion

Considerable efforts have been devoted to overcome fundamental drawbacks associated with molecular imprinting. A common problem is the extensive binding site hetereogeneity associated with the amorphous highly crosslinked MIPs which limits both the rate of mass transfer and the saturation capacity of the materials. Several, more or less laborious approaches have proven successful to address these issues including surface imprinting by immobilized templates and templated synthesis, thin film MIPs by surface initiated polymerization, bead polymerization techniques and nanoparticles allowing chromatographic particle sorting.[1-4]

The advances in controlled radical polymerization for producing linear polymers with defined molecular weights suggests a more direct and simple way to potentially improve the structural properties of MIPs. Sofar the major CRP techniques (RAFT, ATRP, NMP, iniferter) have been investigated as means to achieve this. Most studies report enhanced affinity, binding site accessibility and capacity of the MIP prepared by CRP.[13, 14, 19, 21-24] These results have been mostly discussed in rather general terms referring to the smaller more uniform mesh size created in such networks with no or only minor mention of the pore structure per se. As we have reported here, RAFT polymerization by added CTAs profoundly influences the porous structure of network polymers prepared from a common monomer feed and in a common solvent (Figure 12). Regular FRP in absence of CTA (FRP in toluene) leads to a mesoporous polymer with a very broad distribution of pores featuring low swelling tendency. Several of the binding sites in this network are buried and poorly accessible and hence the chromatographic efficiency is low.

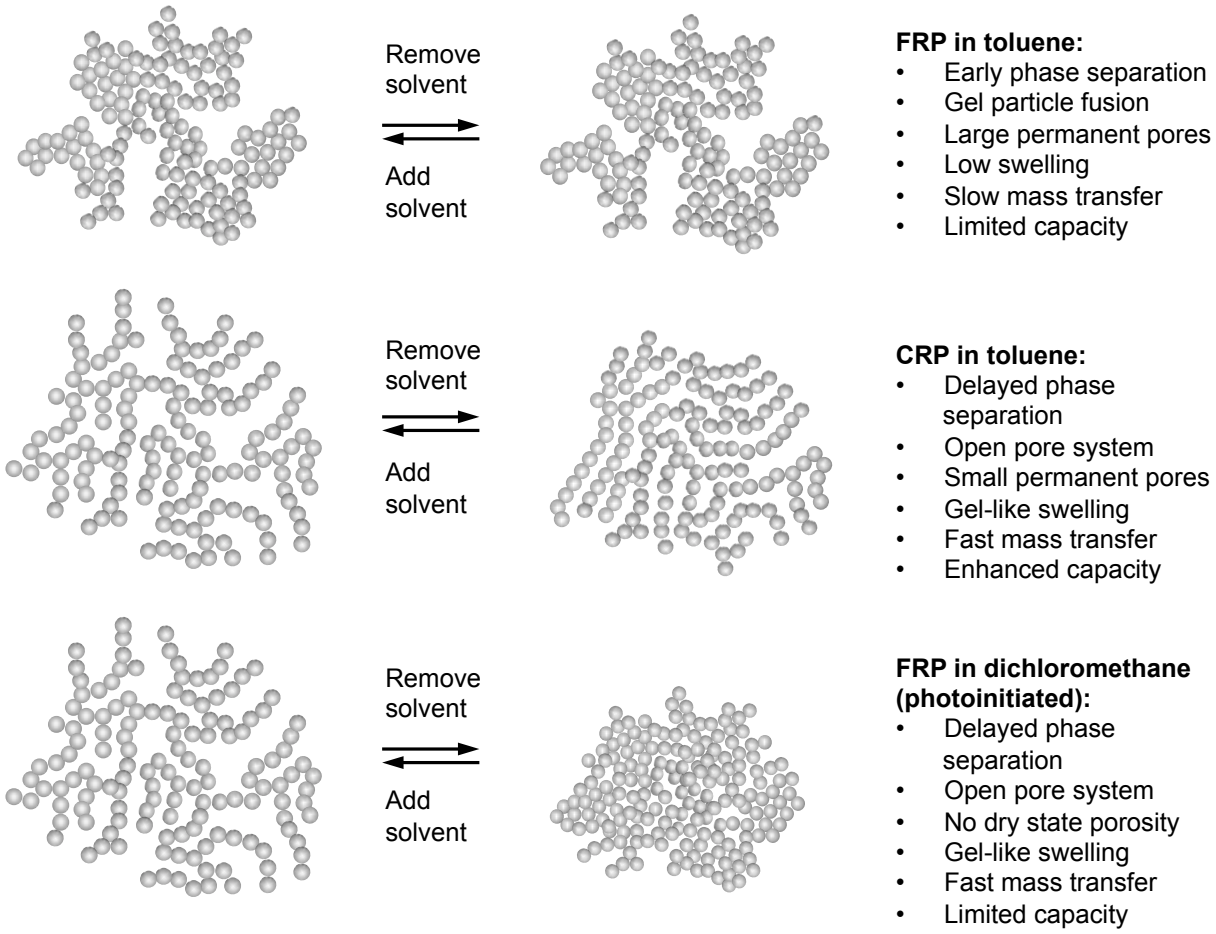

Figure 12. Pore systems arising from different microgel particle connectivities, swelling behaviour and binding properties of imprinted network polymers prepared under different conditions.

Addition of CTA completely changes the picture (CRP in toluene). Given the decreased rate of chain growth and the smaller average size of the primary chains, phase separation is delayed and an open pore structure is formed – this all in analogy with polymers prepared in good solvents or by photoinitated polymerization (FRP in dichloromethane). These polymers swell extensively in good solvents. Interestingly, in the dry state the RAFT polymerized MIP still retains a high specific surface area whereas the photopolymerized MIP prepared by FRP in a good solvent

feature no pores in the dry state. The microgel particle connectivity seems to be more robust for the RAFT polymerized MIP.

These structural effects sufficiently explain the enhanced capacity observed in MIPs prepared by controlled radical polymerization with no need to invoke factors related to network homogeneity per se.

Acknowledgements

The authors wish to acknowledge the financial support from the European Commission under FP7 – Marie Cure Actions, contract PITN-GA-2008-214226 [NEMOPUR].

1. M. J. Whitcombe, N. Kirsch and I. A. Nicholls, *Journal of Molecular Recognition*, 2014, **27**, 297-401.
2. B. Sellergren and A. J. Hall, in *Supramolecular Chemistry: from Molecules to Nanomaterials*, eds. J. W. Steed and P. A. Gale, John Wiley & Sons Ltd, Chichester, UK, 2012, pp. 3255-3282.
3. K. Haupt and C. Ayela, *Molecular Imprinting*, Springer, 2012.
4. G. Vasapollo, R. D. Sole, L. Mergola, M. R. Lazzoi, A. Scardino, S. Scorrano and G. Mele, *International Journal of Molecular Sciences*, 2011, **12**, 5908.
5. B. Sellergren and A. J. Hall, in *Molecularly imprinted polymers. Man-made mimics of antibodies and their applications in analytical chemistry.*, ed. B. Sellergren, Elesevier Science B.V., Amsterdam, 2001, vol. 23, pp. 21-57.
6. B. Sellergren and K. J. Shea, *J. Chromatogr.*, 1993, **635**, 31.

7. K. D. Shimizu, in *Molecularly Imprinted Materials: Science and Technology*, 2005, pp. 419-434.

8. Y. Chen, M. Kele, P. Sajonz, B. Sellergren and G. Guiochon, *Anal. Chem.*, 1999, **71**, 928-938.

9. G. Moad and D. H. Solomon, *The chemistry of free radical polymerization*, Elsevier Science Ltd., Bath, 1995.

10. B. Rückert, A. J. Hall and B. Sellergren, *J. Mat. Chem.*, 2002, **12**, 2275-2280.

11. B. Sellergren, B. Ruckert and A. J. Hall, *Advanced Materials*, 2002, **14(17)**, 1204-1208.

12. M.-M. Titirici and B. Sellergren, *Chemistry of Materials*, 2006, **18**, 1773-1779.

13. M. R. Halhalli, C. S. A. Aureliano, E. Schillinger, C. Sulitzky, M. M. Titirici and B. Sellergren, *Polymer Chemistry*, 2012, **3**, 1033-1042.

14. M. R. Halhalli, E. Schillinger, C. S. A. Aureliano and B. Sellergren, *Chemistry of Materials*, 2012, **24**, 2909-2919.

15. M. R. Halhalli and B. Sellergren, *Chemical Communications*, 2013, **49**, 7111-7113.

16. S. Boonpangrak, M. J. Whitcombe, V. Prachayasittikul, K. Mosbach and L. Ye, *Biosensors & Bioelectronics*, 2006, **22**, 349-354.

17. X. Wei and S. M. Husson, *Ind. Eng. Chem. Res.*, 2007, **46**, 2117-2124.

18. X. Wei, X. Li and S. M. Husson, *Biomacromolecules*, 2005, **6**, 1113-1121.

19. A. D. Vaughan, S. P. Sizemore and M. E. Byrne, *Polymer*, 2007, **48**, 74-81.

20. B. Zu, Y. Zhang, X. Guo and H. Zhang, *J. Polym. Sci., Part A: Polym. Chem.*, 2010, **48**, 532-541.

21. A. D. Vaughan, J. B. Zhang and M. E. Byrne, *AIChE J.*, 2010, **56**, 268-279.

22. V. D. Salian and M. E. Byrne, *Macromolecular Materials and Engineering*, 2013, **298**, 379-390.

23. T. Zhou, L. Jorgensen, M. A. Mattebjerg, I. S. Chronakis and L. Y. Ye, *RSC Advances*, 2014, **4**, 30292-30299.

24. C. Gonzato, P. Pasetto, F. Bedoui, P.-E. Mazeran and K. Haupt, *Polymer Chemistry*, 2014, **5**, 1313-1322.

25. J. Chiefari, Y. K. Chong, F. Ercole, J. Krstina, J. Jeffery, T. P. T. Le, R. T. a. Mayadunne, G. F. Meijs, C. L. Moad, G. Moad, E. Rizzardo and S. H. Thang, *Macromolecules*, 1998, **31**, 5559-5562.

26. J. Pyun and K. Matyjaszewski, *Chem. Mater.*, 2001, **13**, 3446-3448.

27. W. Li, H. Gao and K. Matyjaszewski, *Macromolecules*, 2009, **42**, 927-932.

28. H. Gao, W. Li and K. Matyjaszewski, *Macromolecules*, 2008, **41**, 2335-2340.

29. H. Gao and K. Matyjaszewski, *Progress in Polymer Science*, 2009, **34**, 317-350.

30. Q. Yu, S. Xu, H. Zhang, Y. Ding and S. Zhu, *Polymer*, 2009, **50**, 3488-3494.

31. J. Li, B. Zu, Y. Zhang, X. Guo and H. Zhang, *J. Polym. Sci., Part A: Polym. Chem.*, 2010, **48**, 3217-3228.

32. G. Pan, Y. Zhang, Y. Ma, C. Li and H. Zhang, *Angewandte Chemie International Edition*, 2011, **50**, 1-14.

33. Y. Ma, G. Pan, Y. Zhang, X. Guo and H. Zhang, *Angewandte Chemie*, 2013, **125**, 1551-1554.

34. M. Zhao, C. Zhang, Y. Zhang, X. Guo, H. Yan and H. Zhang, *Chemical Communications*, 2014, **50**, 2208-2210.

35. Z. Adali-Kaya, B. Tse Sum Bui, A. Falcimaigne-Cordin and K. Haupt, *Angewandte Chemie International Edition*, 2015, **54**, 5192-5195.

36. D. J. Keddie, G. Moad, E. Rizzardo and S. H. Thang, *Macromolecules*, 2012, **45**, 5321-5342.

37. A. Goto, K. Sato, Y. Tsujii, T. Fukuda, G. Moad, E. Rizzardo and S. H. Thang, *Macromolecules*, 2001, **34**, 402-408.

38. C. Sulitzky, B. Rückert, A. J. Hall, F. Lanza, K. Unger and B. Sellergren, *Macromolecules*, 2002, **35**, 79-91.

39. C. Li and B. C. Benicewicz, *Journal of Polymer Science Part A: Polymer Chemistry*, 2005, **43**, 1535-1543.

40. Y. Chen, M. Kele, I. Quinones, B. Sellergren and G. Guiochon, *J. Chromatogr.*, 2001, **927**, 1-17.

41. K. Miyazaki and T. Horibe, *Journal of Biomedical Materials Research*, 1988, **22**, 1011-1022.

42. D. C. Sherrington, *Chem. Commun.*, 1998, 2275-2286.

43. Q. Liu, P. Zhang, A. Qing, Y. Lan and M. Lu, *Polymer*, 2006, **47**, 2330-2336.

44. M. R. Landry, *Thermochimica Acta*, 2005, **433**, 27-50.

45. Y. d. Miguel, T. Rohr and D. C. Sherrington, *Polymeric Materials in Organic Synthesis and Catalysis*, 2003, 1-52.

46. F. Lanza, M. Rüther, A. J. Hall and B. Sellergren, *Mat. Res. Soc. Symp. Proc.*, 2002, **723**, M5.6.1-11.

47. H. Liu, X. Zhuang, M. Turson, M Zhang, X. Dong, *J. Sep. Sci.* 2008, 31, 1694-1701.